

See discussions, stats, and author profiles for this publication at: <https://www.researchgate.net/publication/308665367>

Manmade target extraction based on multistage decision and its application for change detection in polarimetric synthetic aperture radar image

Article in *Journal of Electronic Imaging* · September 2016

DOI: 10.1117/1.JEI.25.5.053017

CITATIONS

0

READS

95

5 authors, including:



Runmin Cong

Tianjin University

11 PUBLICATIONS 81 CITATIONS

[SEE PROFILE](#)



Chongyi Li

Tianjin University

16 PUBLICATIONS 83 CITATIONS

[SEE PROFILE](#)



Jiaji He

Tianjin University

8 PUBLICATIONS 6 CITATIONS

[SEE PROFILE](#)

Some of the authors of this publication are also working on these related projects:



Project

underwater image enhancement [View project](#)



Project

Saliency Detection with Different Inputs [View project](#)

Journal of Electronic Imaging

JElectronicImaging.org

Manmade target extraction based on multistage decision and its application for change detection in polarimetric synthetic aperture radar image

Runmin Cong
Ping Han
Chongyi Li
Jiaji He
Zaiji Zhang

Manmade target extraction based on multistage decision and its application for change detection in polarimetric synthetic aperture radar image

Runmin Cong,^a Ping Han,^{b,*} Chongyi Li,^a Jiaji He,^a and Zaiji Zhang^{b,c}

^aTianjin University, School of Electronic Information Engineering, 92 Weijin Road, Nankai District, Tianjin 300072, China

^bCivil Aviation University of China, Tianjin Key Lab for Advanced Signal Processing, 2898 Jinbei Road, Dongli District, Tianjin 300300, China

^cXi'an LeiTong Science and Technology Company Limited, 05 Xibu Road, Chang'an District, Xi'an 710119, China

Abstract. Targets of interest are different in various applications in which manmade targets, such as aircraft, ships, and buildings, are given more attention. Manmade target extraction methods using synthetic aperture radar (SAR) images are designed in response to various demands, which include civil uses, business purposes, and military industries. This plays an increasingly vital role in monitoring, military reconnaissance, and precision strikes. Achieving accurate and complete results through traditional methods is becoming more challenging because of the scattered complexity of polarization in polarimetric synthetic aperture radar (PolSAR) image. A multistage decision-based method is proposed composed of power decision, dominant scattering mechanism decision, and reflection symmetry decision. In addition, the theories of polarimetric contrast enhancement, generalized Y decomposition, and maximum eigenvalue ratio are applied to assist the decision. Fully PolSAR data are adopted to evaluate and verify the approach. Experimental results show that the method can achieve an effective result with a lower false alarm rate and clear contours. Finally, on this basis, a universal framework of change detection for manmade targets is presented as an application of our method. Two sets of measured data are also used to evaluate and verify the effectiveness of the change-detection algorithm. ©2016 SPIE and IS&T [DOI: 10.1117/1.JEI.25.5.053017]

Keywords: polarimetric synthetic aperture radar image; manmade target extraction; multistage decision; change detection.

Paper 16250 received Mar. 27, 2016; accepted for publication Aug. 25, 2016; published online Sep. 26, 2016.

1 Introduction

With the development of remote sensing imaging techniques, an increasing amount of experimental data with wide range and high resolution are acquired. Polarimetric synthetic aperture radar (PolSAR) has become one of the most important branches in remote sensing and has been widely used in many areas. In a PolSAR image, the targets can be classified roughly into two categories: manmade target and natural target. Manmade targets, such as aircraft, tanks, buildings, and ships, play more important roles in military and civil fields than in others.^{1–5} Particularly, manmade targets are the key investigation objects during natural disaster damage evaluation,^{6–8} which is crucial for making rescue and reconstruction plans. Detecting and extracting the manmade targets from input data is the basis for damage evaluation. Therefore, more efforts are necessary for advanced and robust algorithm development. In this paper, we focus on extracting manmade targets using PolSAR data due to its all-time and all-weather imaging characteristics.

Due to the different scattering characteristics between manmade and natural targets, the theory of polarimetric decomposition is an effective tool for manmade target detection. Sato et al.⁹ investigated the polarimetric scattering features of manmade objects and proposed a model-based decomposition. They drew the conclusion that the modified correlation coefficient in the left and right circular polarization basis is useful for detecting manmade targets on rough surfaces. The next year, to improve the accuracy of manmade

target detection in PolSAR images, Sato et al.¹⁰ proposed a modified version of scattering power decomposition by simultaneously introducing nonnegative eigenvalue decomposition and a unitary rotation to the covariance matrix. In addition, some scholars introduced optimal polarization into manmade target extraction and achieved a better result. Cai et al.¹¹ proposed a hybrid target detection algorithm to extract manmade targets in PolSAR images based on three cascaded detectors, which include a span detector, polarimetric whitening filter detector, and optimal polarimetric detector. Experimental results also validated the performance of this method. Xiao et al.¹² proposed an optimization scheme to optimize the coherence between polarimetric channels for PolSAR data and enhance the coherence of manmade targets. Combining this technique with the total backscattered power, a method of manmade target extraction and classification was proposed in that paper.

In addition, azimuth stationarity and Rician distribution are regarded as useful properties for manmade target detection and description. Wu et al.¹³ proposed a new azimuth stationarity extraction method to detect manmade targets in urban areas based on Rician distribution. Xu et al.¹⁴ proposed a manmade target extraction method based on scattering mechanism identification and azimuthal symmetry decision. Inspired by this method, a method based on a multistage decision, which includes power decision, dominant scattering mechanism decision, and reflection symmetry decision, is proposed in this paper. Moreover, the manmade target extraction method

*Address all correspondence to: Ping Han, E-mail: hanpingcauc@163.com

is applied to change detection, which is used to extract the artificial changed regions.

In this paper, we focus on extracting manmade targets through a PolSAR image and study its change detection application. The main contributions are as follows.

1. Polarimetric contrast enhancement (PCE) is introduced to enlarge the contrast between two kinds of targets, and a dominant scattering mechanism extraction method is proposed in this paper to achieve more reasonable results from the dominant scattering mechanism.
2. Considering the geometric and scattering characteristics of manmade targets, a manmade target extraction approach based on a multistage decision is proposed in this work.
3. A universal framework of change detection for manmade targets is presented, which is used to determine the changed manmade targets.

2 Proposed Method

2.1 Basic Principle of Proposed Method

It is universally acknowledged that due to the differences in material and shape, manmade targets differentiate from natural targets. Manmade targets in PolSAR images generally appear with strong coherence; however, the coherence of natural targets is weak, which brings about differences in the scattering mechanism between them. Taking all these characteristics into consideration, a method based on a multistage decision is proposed to extract manmade targets through PolSAR images, which includes power decision, dominant scattering mechanism decision, and reflection symmetry decision. The basis block diagram of our algorithm is shown in Fig. 1.

The algorithm attempts to extract the set of manmade targets; in other words, we should classify the experimental

PolSAR data into two categories: manmade targets and natural targets. In our work, the PolSAR image is classified into four subcategories first: the first class of natural target has weak scattering power, the targets with a double-bounce dominant scattering mechanism are regarded as the first class of manmade target, the rest of the targets with a nondouble-bounce dominant scattering mechanism are divided into the second class of natural targets and the second class of manmade targets based on whether reflection symmetry is satisfied or not. Finally, the first and second classes of manmade targets are merged to produce the final set of manmade targets. The detailed steps of our algorithm can be summarized as follows:

1. Preprocessing. Speckle noise is produced in the SAR images because of the principle of coherent backscattering imaging, which lowers the image quality and has a serious influence on the SAR images. First, the speckle-filtering method¹⁵ is used to reduce the influence of speckle noise. In order to reduce the impact of random orientation on experimental results, orientation angle compensation^{16,17} is also introduced before detection.
2. The power decision. Before conducting the power decision, the PCE procedure is introduced to weaken the influence of the strong scattering points in natural features. After that, the threshold segmentation method is used to determine whether the target belongs to the natural features. That is to say, if the power of a target is lower than a specific threshold (i.e., $\text{span} \leq Th_1$), it should be classified into the first class of natural target; otherwise, proceed to the next step.
3. The dominant scattering mechanism decision. If the target does not satisfy the power decision, this decision should be conducted. According to the dominant scattering mechanism extraction method proposed in Sec. 2.4, the dominant scattering mechanism of the

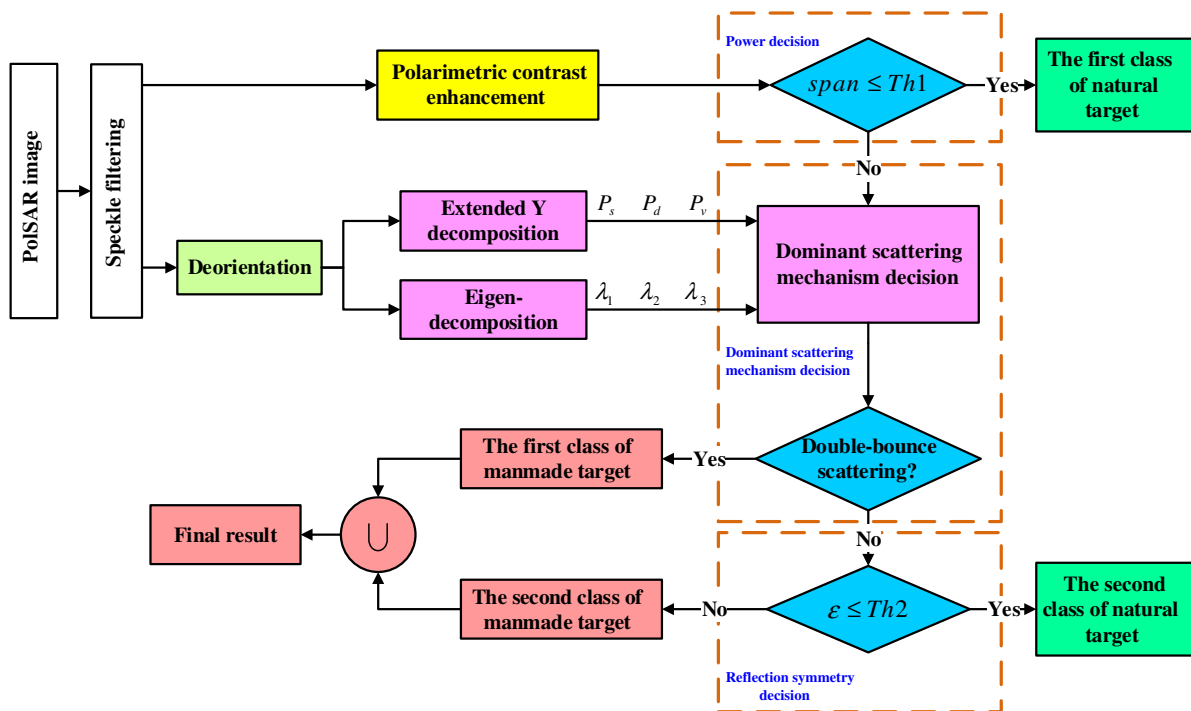


Fig. 1 The principal block diagram of our method.

- target can be determined; then the targets with a double-bounce dominant scattering mechanism will be classified into the first manmade object class. Otherwise, proceed to the reflection symmetry decision.
4. The reflection symmetry decision. The category of the targets that do not satisfy the dominant scattering mechanism decision will be determined based on the reflection symmetry decision. If the target has the characteristic of reflection symmetry, it will be classified into the second class of natural targets; otherwise, it will be put into the second category of manmade targets.
 5. Finally, the first and the second classes of manmade targets are combined into the final manmade target set.

In the following, the basics of a polarimetric matrix, which are of vital importance during the whole algorithm, are introduced in Sec. 2.2. Then, the theory of PCE and a dominant scattering mechanism extraction method are proposed in Secs. 2.3 and 2.4, respectively. Finally, the details of the reflection symmetry decision are presented in Sec. 2.5.

2.2 Basics of the Polarimetric Matrix

There are many representations to describe the polarimetric information of PolSAR images, e.g., complex scattering matrix S , covariance matrix C , coherency matrix T , mueller matrix M , and stokes matrix K . The covariance matrix C under the reciprocity condition is represented as^{7,18}

$$C = \begin{bmatrix} C_{11} & C_{12} & C_{13} \\ C_{12}^* & C_{22} & C_{23} \\ C_{13}^* & C_{23}^* & C_{33} \end{bmatrix} = \left\langle \begin{bmatrix} |S_{HH}|^2 & \sqrt{2}S_{HH}S_{HV}^* & S_{HH}S_{VV}^* \\ \sqrt{2}S_{HV}S_{HH}^* & 2|S_{HV}|^2 & \sqrt{2}S_{HV}S_{VV}^* \\ S_{VV}S_{HH}^* & \sqrt{2}S_{VV}S_{HV}^* & |S_{VV}|^2 \end{bmatrix} \right\rangle, \quad (1)$$

where S_{HH} and S_{VV} produce the power return in the copolarized channels, S_{VH} and S_{HV} produce the power return in the cross-polarized channels, $\langle \dots \rangle$ denotes temporal or spatial ensemble averaging, and C_{ij} is the (i, j) entry of C . The total scattered power SPAN in the case of a polarimetric radar system is defined as the sum of the elements of the principal diagonal of matrix C :

$$\text{SPAN} = C_{11} + C_{22} + C_{33}. \quad (2)$$

The relationship between different matrices is shown in Fig. 2. From this diagram, it is observed that matrices T and C can be converted to each other; that is to say, T and C are equivalent.

2.3 Polarimetric Contrast Enhancement

Generally speaking, manmade targets have strong scattering power in PolSAR images due to their special structure, shape, and material. As a result, the power decision is often introduced in traditional manmade target extraction methods, which excludes some natural targets with weak scattering power. The mainstream decision method is threshold segmentation, and the threshold can be obtained from experience or some automatic methods, such as the constant false alarm rate detection method.¹⁹ However, there are some defects in different methods; for example, people from different backgrounds may achieve different segmentation results based on their subjective experience, and automatic methods always largely depend on the statistical characteristics of experimental data. Sometimes the threshold is not reasonable.

In addition, some natural targets also have strong scattering characteristics due to multiple scattering, such as valleys, mountain forests, lush farmland, and mature tree trunks. The power of different samples is shown in Fig. 3. During the process of the power decision, if the segmentation threshold is set too high, many manmade objects will be classified as natural targets. On the contrary, a smaller threshold will lead to more natural targets entering into subsequent decision processes and increase the difficulty of subsequent judgment. Therefore, we would rather choose a small threshold than selecting a larger one. In this paper, the theory of PCE is introduced before the power decision, which enhances the power of manmade targets and reduces the power of natural targets.

Without loss of generality, we assume target A is strengthened and B is the target to be suppressed. In order to achieve the maximum contrast between A and B, the objective function is defined as follows:^{20–22}

$$\max \left| r_{ab} = \frac{\mathbf{W}^H C_a \mathbf{W}}{\mathbf{W}^H C_b \mathbf{W}} \right|, \quad (3)$$

where r_{ab} denotes the contrast between A and B; the numerator and denominator are the scattering power of targets

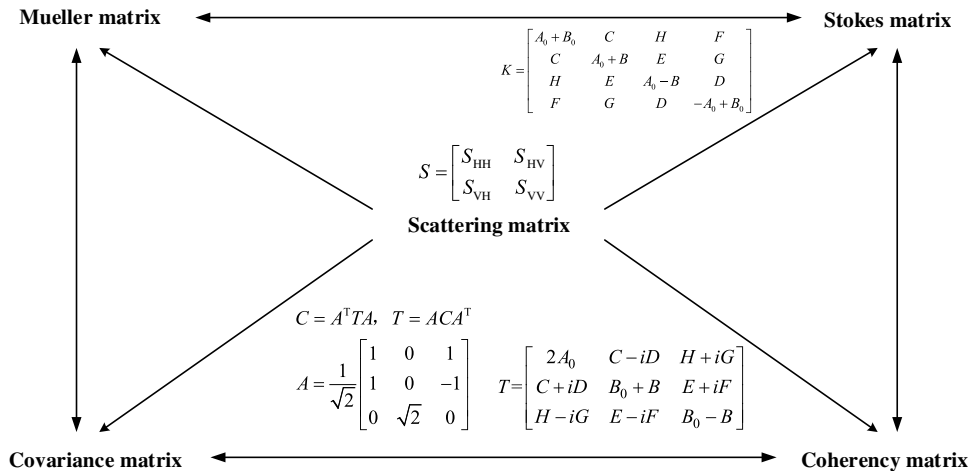


Fig. 2 Relationship of conversion between different matrices.

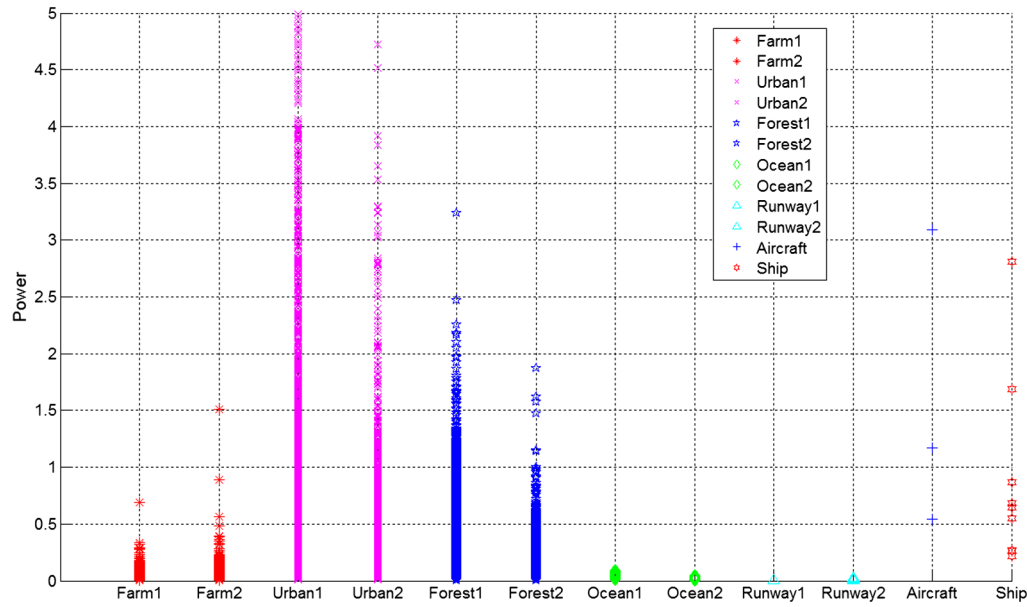


Fig. 3 Power comparison of different samples in Hayward area.

A and B, respectively; and C_a is the polarization covariance matrix of the target.

Using the Lagrange multiplier method, the constraint function is converted to

$$f(\mathbf{W}) = \mathbf{W}^H C_a \mathbf{W} + \lambda [1 - \mathbf{W}^H C_b \mathbf{W}], \quad (4)$$

where $\mathbf{W} = [W_{HH} \ W_{HV} \ W_{VV}]^T$ is the polarization matching vector.

The solution of the gradient vector equation set for the real and imaginary parts of \mathbf{W} can be represented as

$$C_a \mathbf{W} = \lambda C_b \mathbf{W}. \quad (5)$$

As a result, the maximum eigenvalue λ_{\max} of $C_b^{-1} C_a$ is the optimal λ , denoted as λ_{opt} , and the corresponding optimal polarization matching vector is denoted as \mathbf{W}_{opt} . The power intensity of an image can be expressed as

$$\begin{aligned} Y &= [\mathbf{W}_{\text{opt}}^H \bullet \mathbf{X}]^2 = \mathbf{W}_{\text{opt}}^H \bullet \mathbf{X} \bullet \mathbf{X}^H \bullet \mathbf{W}_{\text{opt}} \\ &= \mathbf{W}_{\text{opt}}^H \bullet (\mathbf{X} \bullet \mathbf{X}^H) \bullet \mathbf{W}_{\text{opt}} = \mathbf{W}_{\text{opt}}^H \bullet (C \bullet A) \bullet \mathbf{W}_{\text{opt}}, \end{aligned} \quad (6)$$

where $\mathbf{X} = [S_{HH} \ S_{HV} \ S_{VV}]^T$ and $A = \begin{bmatrix} 1 & 1/\sqrt{2} & 1 \\ 1/\sqrt{2} & \frac{1}{2} & 1/\sqrt{2} \\ 1 & 1/\sqrt{2} & 1 \end{bmatrix}$.

2.4 Dominant Scattering Mechanism Extraction

In terms of scattering mechanisms, there are distinct differences between natural and manmade targets. In general, the dominant scattering mechanism of manmade targets is double-bounce scattering, but some targets, such as trihedral corners, show odd scattering characteristics. In contrast, natural targets have the volume scattering characteristic in most cases, and the double-bounce scattering mechanism is rare.¹⁴ Therefore, we can distinguish manmade targets from natural targets based on the dominant scattering mechanism, and the targets with the double-bounce dominant scattering mechanism will be selected as candidates for manmade targets.

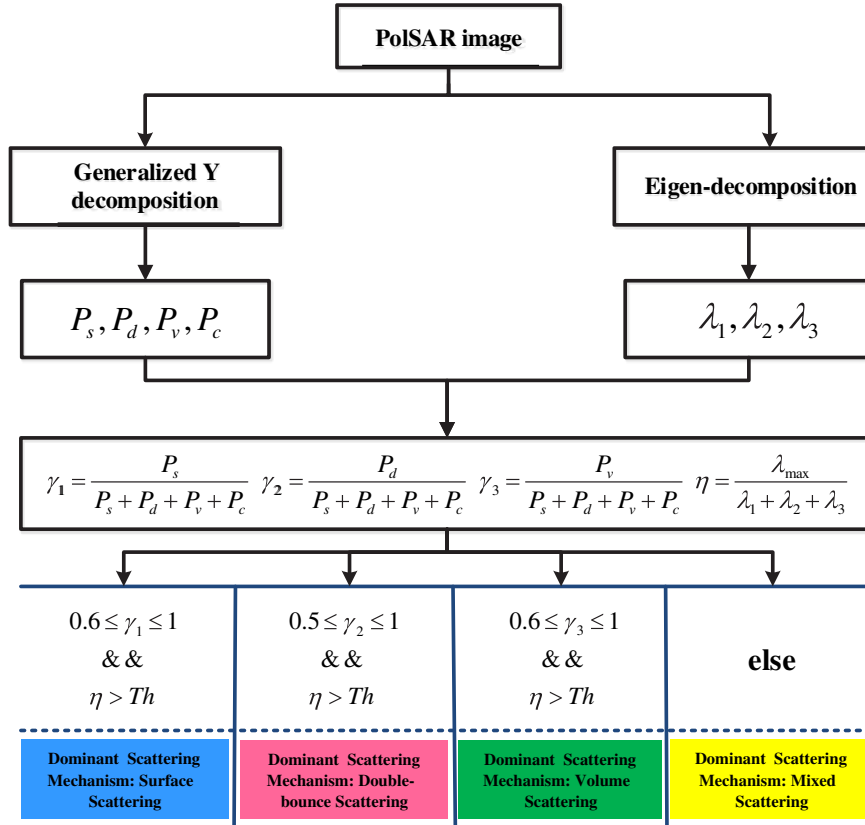
Model-based polarimetric decomposition is a powerful and effective tool for scattering mechanism interpretation.

In Ref. 14, a three-component decomposition method proposed by Freeman and Durden²³ dealing with the reflection symmetry condition that the copolarization and cross-polarization correlations are close to zero is used to extract the dominant scattering mechanism. Nevertheless, this condition is not satisfied in complex urban areas, and Freeman decomposition is inefficient for urban regions. Moreover, Freeman decomposition may produce negative power due to the volume scattering being over-estimated, and it is false in principle. In addition, Xu extracted the dominant scattering mechanism using just the rationale that each component of scattering power accounts for the total scattering power, given the same coefficient for different scattering categories. It is too simple to achieve a comprehensive result.

In order to overcome all the problems mentioned above, a generalized Y decomposition method and a second discriminating factor—the maximum eigenvalue ratio—are introduced. The detailed procedure is shown in Fig. 4. First, generalized Y decomposition²⁴ is introduced to calculate the new four-component scattering power without any constraint condition. At the same time, eigen-decomposition is used to get the eigenvalues for postprocessing. We know that the maximum eigenvalue shows the appearance of the dominant scattering mechanism, and it can be regarded as the supplement of generalized Y decomposition. The maximum eigenvalue ratio is defined as $\eta = \lambda_{\max}/(\lambda_1 + \lambda_2 + \lambda_3)$, where λ_{\max} is the maximum eigenvalue and λ_i denotes the three eigenvalues through eigen-decomposition. Taking the generalized Y decomposition and maximum eigenvalue ratio into account, we can acquire the dominant scattering mechanism of the target. It is worth noting that we arrange different coefficients for different scattering mechanisms, and the threshold for the maximum eigenvalues ratio can be set based on the actual situation, and is generally set to 0.5 to 0.6.

2.5 Reflection Symmetry Decision

For natural targets, there exists an axis of symmetry orthogonal to radar illumination in which the copolarization and the cross-polarization correlations are close to zero, namely,

**Fig. 4** Block diagram of dominant scattering mechanism extraction.

reflection symmetry. However, complex artificial structures can produce strong cross-polarization components or enhance the relevance between copolarization and cross-polarization channels, which causes the condition of reflection symmetry not to be satisfied for manmade targets. Accordingly, the reflection symmetry decision can be used to distinguish manmade targets from natural objects. The parameter of reflection symmetry ϵ is defined as follows:^{14,25}

$$\begin{aligned} \epsilon &= 0.5 \cdot [\text{cor}(S_{\text{HH}}, S_{\text{HV}}) + \text{cor}(S_{\text{HV}}, S_{\text{VV}})], \\ \text{cor}(S_{\text{HH}}, S_{\text{HV}}) &= \frac{\langle S_{\text{HH}} S_{\text{HV}}^* \rangle}{\sqrt{\langle S_{\text{HH}} S_{\text{HH}}^* \rangle \cdot \langle S_{\text{HV}} S_{\text{HV}}^* \rangle}} \\ &= \frac{C_{12}}{\sqrt{C_{11} \cdot C_{22}}} \\ &= \frac{T_{13} + T_{23}}{\sqrt{[T_{11} + T_{22} + 2 \operatorname{Re}(T_{12})] \cdot T_{33}}}, \\ \text{cor}(S_{\text{HV}}, S_{\text{VV}}) &= \frac{\langle S_{\text{HV}} S_{\text{VV}}^* \rangle}{\sqrt{\langle S_{\text{HV}} S_{\text{HV}}^* \rangle \cdot \langle S_{\text{VV}} S_{\text{VV}}^* \rangle}} \\ &= \frac{C_{23}}{\sqrt{C_{22} \cdot C_{33}}} \\ &= \frac{T_{13}^* - T_{23}^*}{\sqrt{[T_{11} + T_{22} - 2 \operatorname{Re}(T_{12})] \cdot T_{33}}}. \end{aligned} \quad (7)$$

The smaller ϵ is, the better orientation characteristic has, and vice versa. If $\epsilon \leq \text{Th2}$, that is to say, the target satisfies reflection symmetry and we should classify it into the natural

target set; otherwise, it should be regarded as a manmade target

$$p_{ij} \in \begin{cases} \text{natural target} & \epsilon \leq \text{Th2} \\ \text{manmade target} & \text{else} \end{cases}, \quad (8)$$

where Th2 is a decision threshold.

3 Experimental Results

3.1 Introduction of Experimental Data

Fully PolSAR data collected by the US AIRSAR system in San Francisco are adopted to evaluate and verify the new algorithm. The detailed parameters of the data are listed in Table 1; the scene includes forests, mountains, parks, urban areas, ocean, grass, bridges, and so on. The Pauli and optical images are shown in Fig. 5.

3.2 Experimental Setup

In the procedure for every decision, we introduced some measures to distinguish the natural targets and manmade targets. Thus, some thresholds are used to make a decision. In fact, we determined these thresholds using some prior knowledge.

In the procedure for the power decision, the threshold Th1 is used to detect the natural targets with lower power values. As described in Sec. 2.1, PCE is introduced to weaken the influence of natural targets with strong scattering power before the power decision in our method. After PCE

Table 1 Introduction of experimental data.

Data information	Data parameters
Acquisition sites	San Francisco, USA
Acquisition system	AIRSAR
Data type	Fully PolSAR data
Size	900 × 1024
Wave band	L-band
Number of looks	4 looks
Range resolution	7.5 m
Azimuth resolution	2 m

operation, the power of some natural targets that have strong scattering characteristics due to multiple scattering, such as valleys, mountain forests, lush farmland, and mature tree trunks, is reduced. Therefore, the threshold can be set to a smaller value in the experiment after PCE, and is generally set to 0.1 to 0.2. In our experiments, it is set to 0.1.

In order to achieve a more reasonable and stable result from the dominant scattering mechanism, the generalized Y decomposition method and a second discriminating factor—the maximum eigenvalue ratio—are introduced in the procedure for dominant scattering mechanism extraction. The condition “ $\eta > Th$ ” is used to make a decision. In all experiments, the threshold Th is set to 0.5.

In the reflection symmetry decision, the parameter ϵ is used to measure the reflection symmetry characteristic of a target. It can be observed from Eq. (8) that the parameter of reflection symmetry is normalized into [0,1]. Without loss of generality, Th2 is set to 0.5 in all of our experiments.

**Fig. 5** Experimental data in San Francisco area: (a) Pauli image and (b) optical image.

3.3 Results

3.3.1 Results of polarimetric contrast enhancement

In the PCE step, we first select some samples according to the different data and applications. In this experiment, the mountain forest regions in the upper-left corner of the input image are selected as the samples to be suppressed, and the urban areas are selected as the sample to be strengthened. Using these samples, PCE is conducted, and the result is shown in Fig. 6. Figure 6(a) shows the original power image of the San Francisco area. It is observed that mountain forest areas (marked in green dashed box) and marine areas located in the upper-right corner of the image (indicated by the red solid-line box) have strong scattering characteristics. In fact, these areas should be regarded as natural areas. After this procedure [shown in Fig. 6(b)], the power of these areas is suppressed on the basis of polarization contrast maximization. Using the enhanced power image, we can achieve a better result for the power decision.

3.3.2 Results of dominant scattering mechanism extraction

Considering the shortcomings of Freeman decomposition, generalized Y decomposition and the maximum eigenvalue ratio are introduced to improve the performance of dominant scattering mechanism extraction. The results are shown in Fig. 7. Xu et al.’s method,¹⁴ shown in Fig. 7(a), classifies more targets, including many urban areas, into the category of volume scattering due to the overestimated volume scattering component, and increases the false alarm rate for post-processing. This problem can be improved in our method, shown in Fig. 7(b); it is rational that the dominant scattering mechanism of the urban area exhibits double-bounce and mixed scattering because of some trees, bungalows, and dihedral angle targets in it. The more precise and reasonable scattering mechanism result we extract, the better manmade extraction results we will achieve.

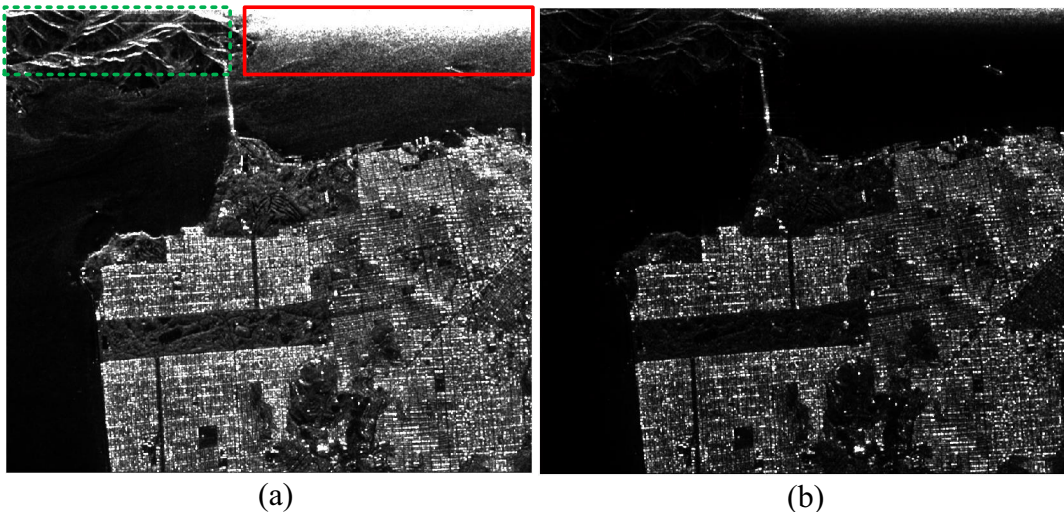


Fig. 6 Power image: (a) power image before PCE and (b) power image after PCE.

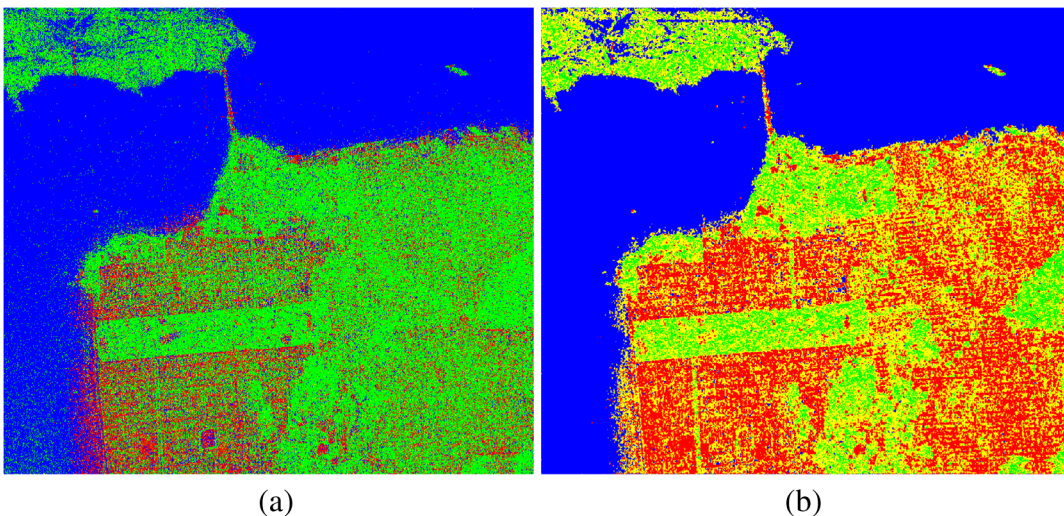


Fig. 7 Results of dominant scattering mechanism extraction. Blue denotes surface scattering, red denotes double-bounce scattering, green denotes volume scattering, and yellow denotes mixed scattering: (a) Xu et al.'s method and (b) our method.

3.3.3 Results of manmade target extraction

In this section, the final manmade target extraction results are shown in Figs. 8 and 9. The results of our method are shown in Fig. 9 with $\text{Th1} = 0.1$ and $\text{Th2} = 0.5$. For fair comparison, the best results of Xu et al.'s method¹⁴ are presented in Fig. 8 with $\text{Th1} = 0.3$ and $\text{Th2} = 0.5$.

Comparing the results of two methods under the precondition of a clear outline for urban areas, Xu et al.'s method cannot avoid the false alarms in marine areas marked as red boxes in Fig. 6. These marine areas with strong scattering, due to their small incident angle and large echo energy, are wrongly classified into the manmade category. If the original power is used directly without any preprocessing, these regions will be reserved until after the power decision and increase the false alarm rate. The forest areas marked with a green dashed box in Fig. 6 face the same problem, which is mainly due to the multiple scattering caused by mountains or trees. If we do nothing for those regions, it will inevitably cause significant interference with manmade

target detection. The method based on the multistage decision proposed in this paper can resolve these problems effectively, which includes PCE and dominant scattering mechanism extraction. By comparison, our method can achieve a better result with a lower false alarm rate and clear outlines.

4 Application in Change Detection

Different application backgrounds have different targets of interest; however, manmade targets (such as buildings, cars, aircraft, ships, and so on) always catch our attention. Change detection methods for manmade targets can be used in many fields like rescuing, urban monitoring, and attack effect evaluation. Thonnessen et al.²⁶ used the structure matching method based on the Hausdorff distance to extract manmade targets for change detection, but it is largely dependent on the process of segmentation. Li et al.²⁷ proposed a framework for detecting urban changes from a pair of very high resolution (VHR) satellite images.

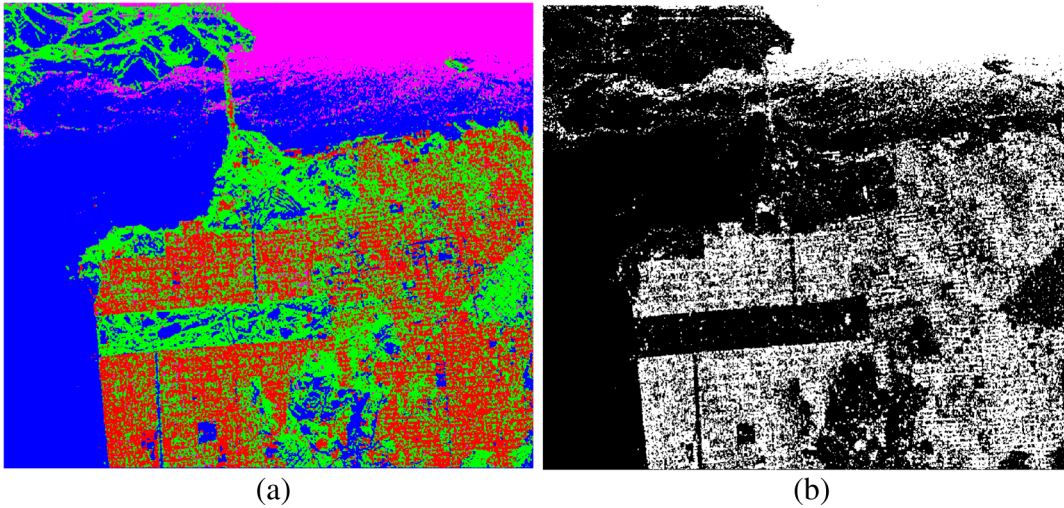


Fig. 8 Results of manmade target extraction using Xu et al.’s method: (a) four categories of targets are represented in different colors. Blue represents the first category of natural targets, green the second category of natural targets, red the first category of manmade targets, and magenta the second category of manmade targets. (b) Binary map in which white denotes manmade targets and black is natural targets.

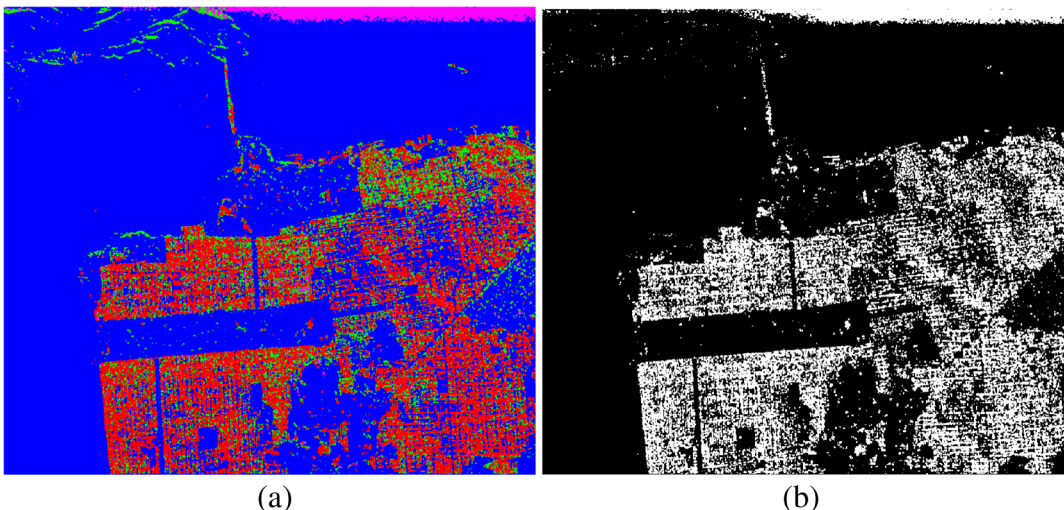


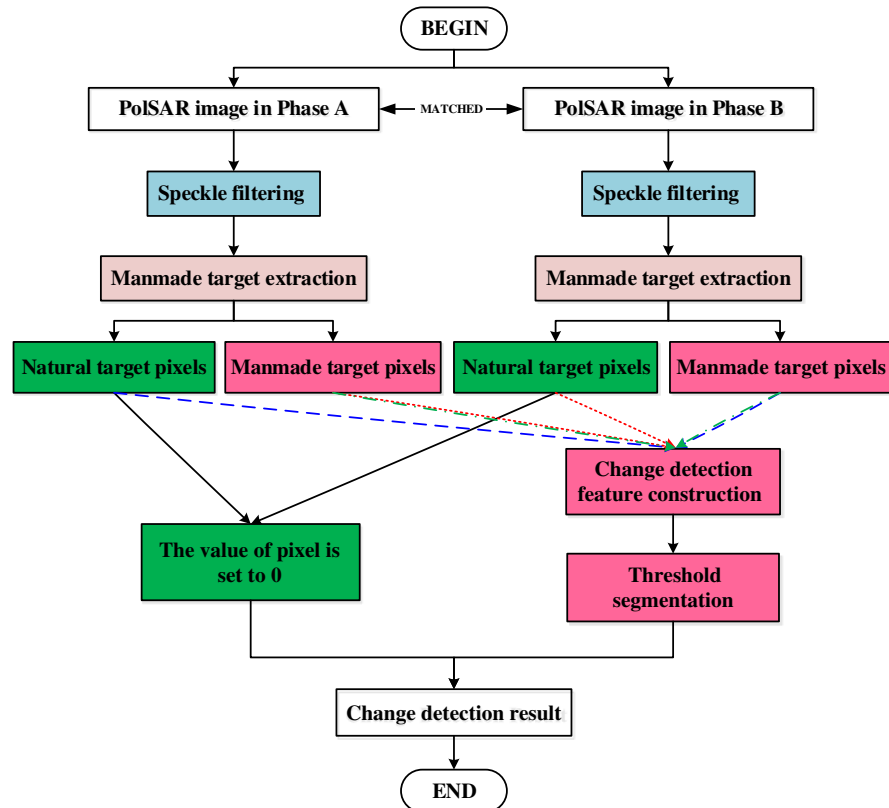
Fig. 9 Results of manmade target extraction using our method: (a) four categories of targets are represented in different colors. Blue indicates the first category of natural targets, green the second category of natural targets, red the first category of manmade targets, and magenta the second category of manmade targets. (b) Binary map in which white denotes manmade targets and black is natural targets.

First, the changed edges in two images are extracted directly, then some shadow regions are excluded to obtain the true changed edges. Based on these edges, the manmade targets can be localized. This method can achieve a better result under VHR conditions, and the two images should be matched accurately. In this section, a universal framework of change detection for manmade targets using PolSAR images is proposed.

4.1 Proposed Method

The flowchart of our method is shown in Fig. 10. It is noteworthy that the feature construction method for change detection can be selected from the existing algorithms, such as polarization likelihood-ratio,¹⁹ joint weighted

polarization difference degree,²⁸ polarization state extraction,²⁹ Wishart distance measure,³⁰ and so on. First, speckle filtering¹⁵ and orientation angle compensation^{16,17} are introduced to reduce the influence of speckle noise and random orientation on experimental results. Next, the manmade target extraction method proposed in Sec. 3 is used to extract the set of natural and manmade targets for two phases of matched PolSAR data. The corresponding pixels that belong to the natural target category in both phases are set to 0; that is to say, we only focus on the changes in manmade regions. As a consequence, the changes in natural regions can be removed. Then, the characteristic for change detection will be calculated using an existing method, and the polarization likelihood-ratio algorithm¹⁹ is chosen in this paper. Finally, threshold segmentation is taken to acquire the binary

**Fig. 10** The flowchart of our change detection method.

result for these pixels and combined with the former zero pixels, which are regarded as natural targets, and the final result appears.

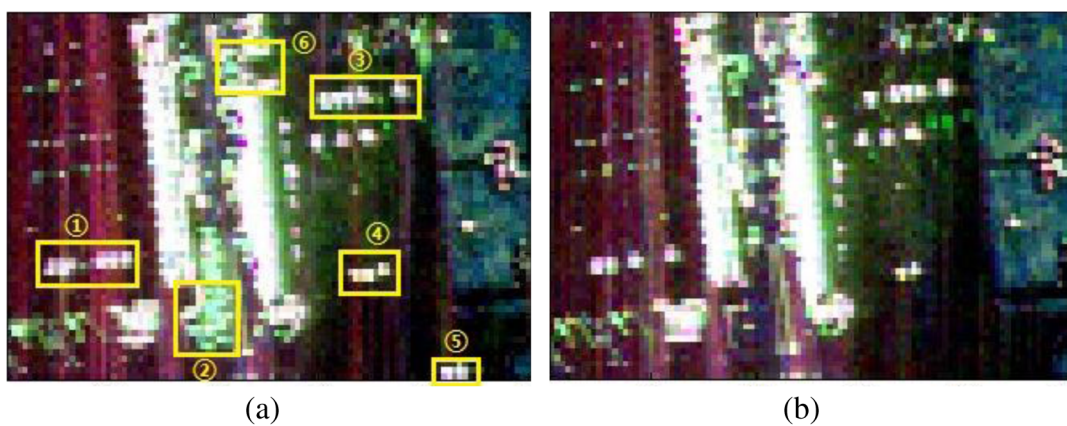
4.2 Experimental Results of Change Detection

4.2.1 Results of airport data in Fresno County

To illustrate the effectiveness of our change detection method, L-band fully PolSAR data collected by the UAVSAR system in Fresno County on May 19, 2011, and May 20, 2011, are used. The two Pauli images are shown in Fig. 11. There are some aircraft, aprons, and hangars; a large number of cars; and a small amount of vegetation in the scene. In Fig. 11, six

obviously changed regions are marked as yellow boxes, which consist of four manmade changed regions (i.e., regions ①, ③, ④, and ⑤).

The relevant results are shown in Figs. 12–14. Manmade target extraction results for both phases are shown in Fig. 12. The difference map is a direct description of change detection, which describes the difference between two PolSAR images. The pixels with large values in the difference map show a greater difference between two PolSAR images, which indicates a high likelihood of change. Figure 13 shows the difference map of the two methods; it is observed that our method detects manmade changed areas successfully and many natural interference regions are removed. The map

**Fig. 11** Airport data in Fresno County: (a) Pauli image on May 19, 2011, and (b) Pauli image on May 20, 2011.

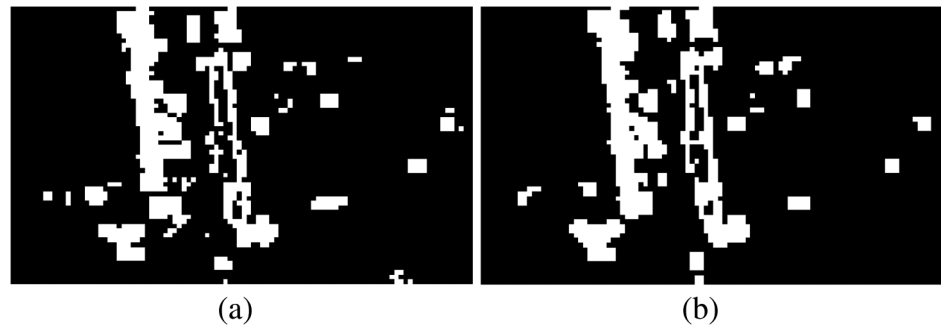


Fig. 12 Results of manmade target extraction using our method: (a) extraction results on May 19, 2011, and (b) extraction results on May 20, 2011.

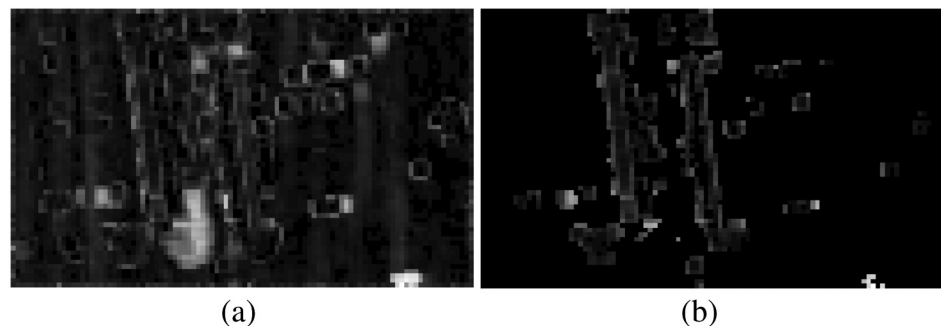


Fig. 13 (a) Difference map of Ref. 19 and (b) difference map of our method proposed in Sec. 4.

after threshold segmentation is shown in Fig. 14, where the threshold is set to 0.13. We can see that the manmade changed regions marked in Fig. 11 are detected with exact locations, but there are some false alarms in the region of the red dotted box, which contains many scattered cars. Therefore, it is difficult to give an objective and precise assessment for them. However, other manmade changed regions can be detected effectively.

4.2.2 Results of airport data in Everglades City

In this section, L-band fully PolSAR data collected by the AIRSAR system in Everglades City on June 15, 2009, and June 22, 2010, are used to evaluate our method. Their Pauli images are shown in Fig. 15, and the closest optical maps

obtained from Google Earth are shown in Fig. 16. There are two manmade changed regions: a building construction changed region marked with a red solid box and an urban changed region marked with a blue oval. Manmade target extraction results in both phases are shown in Fig. 17. Difference maps of the two methods and the final result after threshold segmentation (threshold is set to 0.15) are shown in Figs. 18 and 19, respectively. The manmade changed regions are detected, and some natural changed areas are excluded effectively. However, some regions such as strong noises are reserved as false alarms, and future work should be done to process this problem.



Fig. 14 Final result after threshold segmentation using our method.

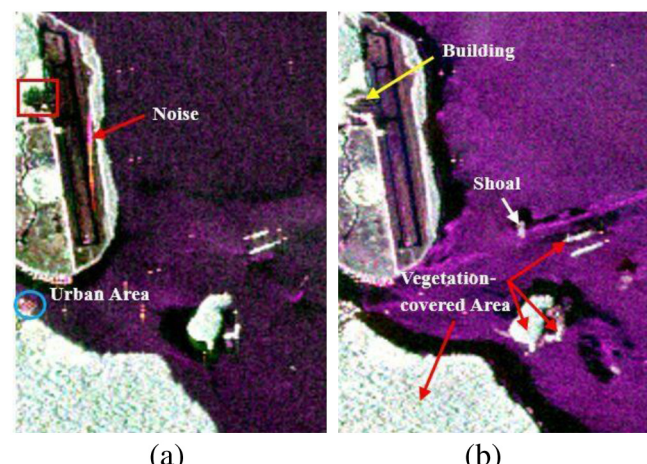


Fig. 15 Airport data in Everglades City: (a) Pauli image on June 15, 2009, and (b) Pauli image on June 22, 2010.



Fig. 16 Optical image of airport data in Everglades City: (a) optical image on January 31, 2009, and (b) optical image on January 23, 2010.

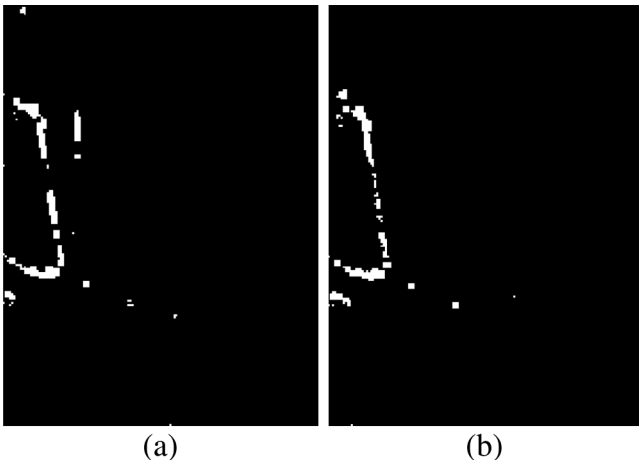


Fig. 17 Results of manmade target extraction using our method: (a) extraction results on June 15, 2009, and (b) extraction results on June 22, 2010.

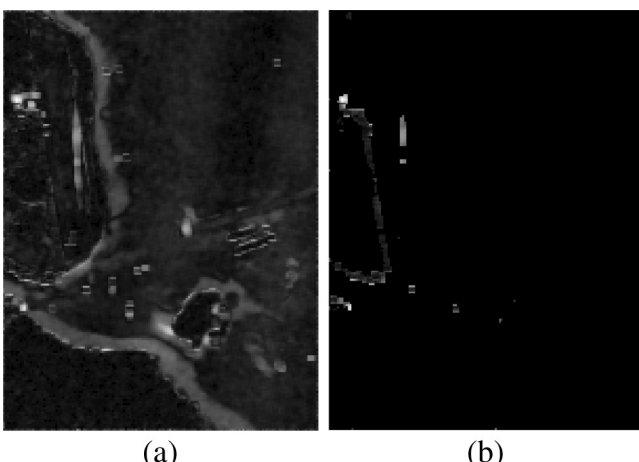


Fig. 18 (a) Difference map of Ref. 19 and (b) difference map our method proposed in Sec. 4.

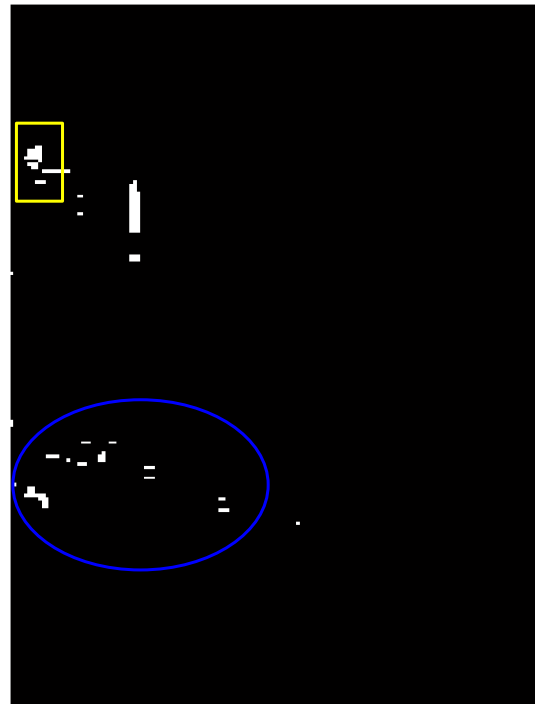


Fig. 19 Final result after threshold segmentation using our method.

5 Conclusion

In this work, a multistage decision method is proposed to extract manmade targets in PolSAR images. Three decision mechanisms are used to achieve an accurate and complete result. In the algorithm, the theory of PCE is introduced to assist the power decision, and a dominant scattering mechanism extraction method, which combines generalized Y decomposition and the maximum eigenvalue ratio, is added to acquire a more robust and reasonable dominant scattering mechanism. In addition, a universal framework of change detection for manmade target is proposed, which is regarded as an application of our manmade target extraction method. Full PolSAR measured data is adopted to evaluate and verify the algorithm. Experimental results show that the method can achieve an effective result with a lower false alarm rate and clear outlines. However, there are some drawbacks to the proposed algorithm. As such, it is important to pay more attention in order to reduce the false alarms and improve robustness in the future. In addition, the intelligent way to determine the thresholds used in the decision stages and comprehensive manmade target extraction method should be further studied.

Acknowledgments

This research work was jointly supported by grants from the National Natural Science Foundation of China (Project Nos. 61571442 and 61471365) and the National Natural Science Foundation of China (Key Program) (Project No. 61231017).

References

1. N. Wang et al., "Polarimetric SAR target detection using the reflection symmetry," *IEEE Geosci. Remote Sens. Lett.*, 9(6), 1104–1108 (2012).
2. N. Wang et al., "Polarimetric SAR target detection based on polarization synthesis," in *Proc. Int. Geoscience and Remote Sensing Symp.*, pp. 5899–5902 (2012).

3. X. Zhang et al., "A novel polarimetric SAR ship detection filter," in *Proc. IET Int. Conf. on Radar*, pp. 1–5 (2013).
4. D. Velotto, M. Soccorsi, and S. Lehner, "Azimuth ambiguities removal for ship detection using full polarimetric X-band SAR data," *IEEE Trans. Geosci. Remote Sens.* **52**(1), 76–88 (2014).
5. P. Han et al., "Runways detection based on scattering similarity and structural characteristics," in *Proc. Conf. on Integrated Communication, Navigation, and Surveillance*, pp. 1–8 (2015).
6. L. Liu et al., "Building footprint extraction by fusing dual-aspect SAR images," in *Proc. Int. Geoscience and Remote Sensing Symp.*, pp. 1866–1869 (2011).
7. Y. Yamaguchi, "Disaster monitoring by fully polarimetric SAR data acquired with ALOS-PALSAR," *Proc. IEEE* **100**(10), 2851–2860 (2012).
8. S. W. Chen and M. Sato, "Tsunami damage investigation of built-up areas using multi-temporal spaceborne full polarimetric SAR images," *IEEE Trans. Geosci. Remote Sens.* **51**(4), 1985–1997 (2013).
9. R. Sato, Y. Yamaguchi, and H. Yamada, "FDTD polarimetric scattering analysis for detection of stricken man-made object," in *Proc. Int. Asia-Pacific Conf. on Synthetic Aperture Radar*, pp. 1–4 (2011).
10. R. Sato et al., "Stricken man-made object detection using scattering power decomposition with NNED and rotation of the covariance matrix," in *Proc. Int. Geoscience and Remote Sensing Symp.*, pp. 5121–5124 (2012).
11. C. Cai, W. T. An, and J. Yang, "A hybrid manmade-target detection algorithm for polarimetric SAR images," in *Proc. IET Int. Conf. on Radar*, pp. 1–5 (2009).
12. S. P. Xiao et al., "Polarimetric coherence optimization and its application for manmade target extraction in PoSAR data," *IEICE Trans. Electron.* **E97-C**(6), 566–574 (2014).
13. W. J. Wu, H. D. Guo, and X. W. Li, "Man-made target detection in urban areas based on a new azimuth stationarity extraction method," *IEEE J. Sel. Top. Appl. Earth Obs. Remote Sens.* **6**(3), 1138–1146 (2013).
14. M. Xu et al., "Man-made target extraction based on scattering mechanism identification and azimuthal symmetry decision of POLSAR images," *J. Natl. Univ. Defense Technol.* **30**(5), 68–72 (2008).
15. J. S. Lee et al., "Scattering-model-based speckle filtering of polarimetric SAR data," *IEEE Trans. Geosci. Remote Sens.* **44**(1), 176–187 (2006).
16. W. T. An, Y. Cui, and J. Yang, "Three-component model-based decomposition for polarimetric SAR data," *IEEE Trans. Geosci. Remote Sens.* **48**(6), 2732–2739 (2010).
17. J. S. Lee and T. L. Ainsworth, "The effect of orientation angle compensation on coherency matrix and polarimetric target decompositions," *IEEE Trans. Geosci. Remote Sens.* **49**(1), 53–64 (2011).
18. J. S. Lee and E. Pottier, *Polarimetric Radar Imaging: From Basics to Applications*, CRC Press, Florida (2009).
19. K. Conradsen et al., "A test statistic in the complex wishart distribution and its application to change detection in polarimetric SAR data," *IEEE Trans. Geosci. Remote Sens.* **41**(1), 4–19 (2003).
20. J. G. Yang et al., "Generalized optimization of polarimetric contrast enhancement," *IEEE Geosci. Remote Sens. Lett.* **1**(3), 171–174 (2004).
21. H. M. Hao and Y. H. Zhang, "The application of optimal polarization theory in polarimetric SAR change detection," in *Proc. Int. Conf. on Multimedia Technology*, pp. 1–3 (2010).
22. J. J. Yin et al., "The use of a modified GOPCE method for forest and nonforest discrimination," *IEEE Geosci. Remote Sens. Lett.* **12**(5), 1076–1080 (2015).
23. A. Freeman and S. L. Durden, "A three-component scattering model for polarimetric SAR data," *IEEE Trans. Geosci. Remote Sens.* **36**(3), 963–973 (1998).
24. G. Singh, Y. Yamaguchi, and S. E. Park, "General four-component scattering power decomposition with unitary transformation of coherency matrix," *IEEE Trans. Geosci. Remote Sens.* **51**(5), 3014–3022 (2013).
25. T. Moriyama et al., "A study on extraction of urban areas from polarimetric synthetic aperture radar image," in *Proc. Int. Geoscience and Remote Sensing Symp.*, pp. 703–706 (2004).
26. U. Thonnessen, G. Hofele, and W. Middelmann, "Change detection in satellite images," *Proc. SPIE* **5809**, 197 (2005).
27. W. M. Li et al., "A novel framework for urban change detection using VHR satellite images," in *Proc. Int. Conf. on Pattern Recognition*, pp. 312–315 (2006).
28. P. Han and R. M. Cong, "Change detection algorithm of polarimetric SAR image based on joint weighted polarization difference degree," *J. Signal Process.* **29**(10), 1390–1397 (2013).
29. P. Han, R. M. Cong, and Z. J. Zhang, "Change detection algorithm of polarimetric SAR image based on polarization state extracting," *Syst. Eng. Electron.* **37**(7), 1526–1530 (2015).
30. M. Liu et al., "Change detection of polarimetric SAR images applied to specific land cover type," in *Proc. Int. Geoscience and Remote Sensing Symp.*, pp. 6329–6332 (2012).

Runmin Cong received his MS degree from the Civil Aviation University of China (CAUC), Tianjin, China, in 2014. He is currently pursuing his PhD at the School of Electronic Information Engineering, Tianjin University (TJU), Tianjin, China. His research interests include SAR image processing, 3-D imaging, and computer vision.

Ping Han received his PhD from TJU, Tianjin, China, in 2004. She is currently a professor with the School of Electronic Information and Automation, CAUC, Tianjin, China. Her current research interests include SAR image processing, target detection, and pattern recognition.

Chongyi Li is pursuing his PhD at the School of Electronic Information Engineering in TJU, Tianjin, China. His current research focuses on digital image processing, signal processing, and computer vision.

Jiaji He is now pursing his PhD degree at the School of Electronic Information Engineering in TJU, Tianjin, China. His current research focuses on IC design and relevant preprocessing algorithms.

Zaiji Zhang received her MS degree from CAUC, Tianjin, China. Her research interests include SAR image processing and change detection.